Spectranalyzed) solution onto an aqueous [water from a Milli-Q (Millipore Corporation, Bedford, MA) system was used] subphase in a commercial NIMA (Warwick Science Park, Coventry, England) trough. The subphase water included 5×10^{-4} M $ZnCl_2$ (Aldrich, 99.99%) and was adjusted to a pH of 6.5 to 7 by addition of NaOH (Aldrich, 99%). Substrates were freshly cleaved mica or polished Si wafers (Semiconductor Processing, Boston, MA) [orientation (100), 3 ohm-cm, *n*-type with a root mean square roughness of ~3 Å as measured by an AFM]. Before deposition, the Si wafers were cleaned in a hot solution of H_2O_2-H_2SO_4 (3:7 ratio) to remove any organic contaminants while leaving the amorphous native oxide intact, then stored in clean water until use. The mica substrates were cleaned by continuous rinsing with ethanol for 5 min. After removal from the ethanol bath, we cleaved the mica, using ordinary adhesive tape, and inserted it into the subphase. LB films were deposited at a surface pressure of 30 mN/m at 22.0° ± 0.5°C.

13. Resolution in our AFM images was assessed as follows. We evaluated the degree of drift in the image by comparing FTs of images scanned in opposite directions (up and down). The initial variations between spot positions from up and down scans were often as large as 0.1 nm in position and 3° in angle. However, after scanning times on a single area ranging from 0.5 to 2 hours, Fourier spots from the two scan directions were in the same location within our ability to measure them, given the digitization of the data on the display (0.01 nm, 0.5°). No damage was done to the sample even after hours of continuous imaging. We examined each sample with several AFM tips to eliminate any systematic errors arising from multiple or asymmetric tips. Typical forces were estimated to be 10^{-8} N. This protocol was essential to ensure that the disorder present in images of the hexatic films was a result of the film disorder and not thermal drift or hysteresis in the piezo drivers. A detailed discussion of AFM calibration, errors, and reproducibility is presented elsewhere (*10*).
14. The approximate tilt angle that maximizes close packing for an all-*trans* alkane chain is tan θ = *R*/*D*, where *R* is the next nearest carbon spacing in the all-*trans* chain, 2.5 to 2.6 Å, and *D* is the separation between molecules, about 4.7 to 4.8 Å for nearest neighbors in this lattice. For nearest neighbors, the first tilt is ≈28°, which is consistent with the tilt angle suggested by the ratio of the two lattice vectors, cos θ = 0.48/0.56, about 31°, and the ratio of the measured bilayer thickness of 4.7 nm to the extended length of an arachidic acid bilayer of 5.5 nm, or cos θ = 4.7/5.5, about 30°.
15. A. I. Kitaigorodskii, *Organic Chemical Crystallography* (Consultant Bureau, New York, 1961).
16. J. M. Kosterlitz and D. J. Thouless, *J. Phys. C* **5**, L124 (1972); *ibid.* **6**, 1181 (1973).
17. B. I. Halperin and D. R. Nelson, *Phys. Rev. Lett.* **41**, 121 (1978); *ibid.*, p. 519; D. R. Nelson and B. I. Halperin, *Phys. Rev. B* **19**, 2457 (1979).
18. For an excellent summary of the theoretical and experimental work in this area, see K. J. Strandburg, Ed., *Bond Orientational Order in Condensed Matter Systems* (Springer-Verlag, New York, 1992).
19. C. A. Murray and D. H. Van Winkle, *Phys. Rev. Lett.* **58**, 1200 (1987); C. A. Murray and R. A. Wenk, *ibid.* **62**, 1643 (1989).
20. R. J. Birgeneau and J. D. Litster, *J. Phys. (Paris) Lett.* **39**, L-399 (1978); J. D. Brock *et al.*, *Phys. Rev. Lett.* **57**, 98 (1986).
21. R. Pindak, D. E. Moncton, S. C. Davey, J. W. Goodby, *Phys. Rev. Lett.* **46**, 1135 (1981); M. Cheng, J. T. Ho, S. W. Hui, R. Pindak, *ibid.* **59**, 1112 (1987).
22. J. Maclennan and M. Seul, *ibid.* **69**, 2082 (1992).
23. X. Qiu *et al.*, *ibid.* **67**, 703 (1991); J. V. Selinger, Z.-G. Wang, R. F. Bruinsma, C. M. Knobler, *ibid.* **70**, 1139 (1993).
24. K. Kjaer *et al.*, *ibid.* **58**, 2224 (1987); C. A. Helm, H. Mohwald, K. Kjaer, J. Als-Nielsen, *Biophys. J.* **52**, 381 (1987).
25. D. R. Nelson, M. Rubenstein, F. Spaepen, *Philos. Mag. A* **46**, 105 (1982).
26. H. Dai, H. Chen, C. M. Lieber, *Phys. Rev. Lett.* **66**, 3183 (1991); H. Dai and C. M. Lieber, *ibid.* **69**, 1576 (1992); *J. Phys. Chem.* **97**, 2362 (1993).
27. D. J. Bishop, P. L. Gammel, D. A. Huse, C. A. Murray, *Science* **255**, 165 (1992); C. A. Murray *et al.*, *Phys. Rev. Lett.* **64**, 2312 (1990).
28. E. M. Chudnovsky, *Phys. Rev. B* **40**, 11355 (1989).
29. M. C. Marchetti and D. R. Nelson, *ibid.* **41**, 1910 (1990).
30. M. Prakash, J. B. Peng, J. B. Ketterson, P. Dutta, *Chem. Phys. Lett.* **128**, 354 (1986).
31. We thank D. R. Nelson for his suggestion that the substrate could be the source of defects and C. Knobler, E. Sirota, and R. Pindak for discussions on Langmuir films, rotator phases, and hexatics. We thank C. Jeppeson and J. Woodward for help with the image analysis software and F. Grunfeld for technical assistance with the LB trough. This work was supported by Office of Naval Research grant N00014-90-J-1551, NSF grant CTS-9305868, NIH grants GM47334 and HL51177, and the Materials Research Laboratories (MRL) Central Facilities supported by NSF under award DMR-9123048.

1 February 1995; accepted 27 April 1995

Synthesis and Structure of an Iron(III) Sulfide–Ferritin Bioinorganic Nanocomposite

Trevor Douglas,* Dominic P. E. Dickson, Steven Betteridge, John Charnock, C. David Garner, Stephen Mann†

Amorphous iron sulfide minerals containing either 500 or 3000 iron atoms in each cluster have been synthesized in situ within the nanodimensional cavity of horse spleen ferritin. Iron-57 Mössbauer spectroscopy indicated that most of the iron atoms in the 3000–iron atom cores are trivalent, whereas in the 500–iron atom clusters, approximately 50 percent of the iron atoms are Fe(III), with the remaining atoms having an effective oxidation state of about +2.5. Iron K-edge extended x-ray absorption fine structure data for the 500–iron atom nanocomposite are consistent with a disordered array of edge-shared FeS_4 tetrahedra, connected by $Fe(S)_2Fe$ bridges with bond lengths similar to those of the cubane-type motif of iron-sulfur clusters. The approach used here for the controlled synthesis of bioinorganic nanocomposites could be useful for the nanoscale engineering of dispersed materials with biocompatible and bioactive properties.

The nanoscale synthesis of inorganic particles is currently of great interest in materials chemistry (*1*). One possible route to the preparation of such materials involves the use of preorganized biomolecular architectures as chemically and spatially confined environments for the construction of inorganic clusters and nanoparticles (*2*). The 8-nm polypeptide cage of the Fe storage protein ferritin has been used to prepare nanocomposites containing pure phases of magnetite [Fe_3O_4 (magnetoferritin)] (*3*), amorphous uranium oxide (*4*), and amorphous MnOOH (*4*, *5*). An advantage of this biomimetic approach is that the inorganic nanoscale materials can be rendered biocompatible by virtue of their intimate association with the surrounding polypeptide assembly. Thus, if appropriate synthetic routes could be developed, bioinorganic nanoparticles might be useful as biological sensors and markers, drug carriers, and diagnostic and bioactive agents. For example, magnetoferritin shows potential as a contrast agent for magnetic resonance imaging of tissue (*6*) and uranium oxide–loaded ferritin could have use in neutron-capture therapy (*7*).

The synthesis of metal sulfides within ferritin could be a feasible route to the controlled construction of semiconductor and nonstoichiometric particles with technological, and perhaps biological, importance. The transformation of the hydrated iron(III) oxide [ferrihydrite ($FeOOH{\cdot}nH_2O$)] core of native ferritin to an iron sulfide has been investigated under alkaline (pH 8.9) reaction conditions (*4*, *8*). Electron diffraction (*4*) and ^{57}Fe Mössbauer spectroscopy (*8*) indicated that the product consisted of a thin surface coating of amorphous iron(II) sulfide on an essentially unmodified crystalline ferrihydrite core.

In this report, we describe a method for the in situ synthesis of iron sulfides in ferritin that results in the complete transformation of native or reconstituted iron oxide cores. An approach involving demetallation, reconstitution, and chemical reaction allows control over the particle size. The reaction product is a highly unusual amorphous sulfide consisting predominantly of trivalent Fe; insight into the local structure has been gained by extended x-ray absorption fine structure (EXAFS) analysis, a

T. Douglas and S. Mann, School of Chemistry, University of Bath, Bath BA2 7AY, UK.
D. P. E. Dickson and S. Betteridge, Department of Physics, University of Liverpool, Liverpool L69 3BX, UK.
J. Charnock, Daresbury Laboratory, Warrington, Cheshire WA4 4AD, UK.
C. D. Garner, Department of Chemistry, University of Manchester, Manchester M13 9PL, UK.

*Present address: Department of Biological and Physical Sciences, Montana State University, Billings, MT 58101, USA.
†To whom correspondence should be addressed.

technique that has been used successfully to probe the local environments of metals in ferritin (9).

Addition of aqueous sodium sulfide under an Ar atmosphere to acidic (pH = 5.4) solutions of native horse spleen ferritin (3000 Fe atoms per molecule) resulted in a distinct color change from yellow-brown to dark green (*10*). Ultraviolet-visible spectra showed the formation of a new material that exhibited absorption maxima at 426 and 338 nm (Fig. 1). These spectra are similar to the visible absorption spectra of cluster compounds such as $[Fe_4S_4(SR)_4]^{2-}$ and $[Fe_2S_2(SR)_4]^{2-}$ (R, alkyl) (*11*). The reaction was rapid and reached steady state after approximately 40 min. At this stage the reaction solution was homogeneous, but after roughly 48 hours, in the presence of excess sulfide, some precipitation was evident. Removal of the excess sulfide by dialysis against deaerated acetate buffer (pH 5.4) markedly increased the stability of the nanocomposite in the absence of air. Transmission electron microscopy (TEM) of the transformed native ferritin (*12*) showed discrete electron-dense cores ~6.5 nm in diameter (Fig. 2), similar in size to the unreacted ferritin biomineral. The sulfided cores exhibited no discernible electron diffraction reflections, whereas the unreacted ferritin cores showed six lines corresponding to the mineral ferrihydrite. Energy-dispersive x-ray analysis (EDXA) showed that the amorphous ferritin cores contained Fe and S.

Reaction of a solution of reconstituted ferritin containing ferrihydrite cores of ~500 Fe atoms per molecule (*13*) with an acidic sulfide solution also resulted in the formation of a homogeneous deep green sol. TEM images showed that the reaction product consisted of discrete irregular particles of <2 nm that showed no evidence of crystallinity by electron diffraction and, according to EDXA, contained both Fe and S. The EXAFS analysis of the sulfided sample (*14*) showed that the Fe atoms were coordinated to four S atoms at 2.22 Å, with no evidence for O or other light atoms in the first coordination shell (Fig. 3A). The Fourier transform of the EXAFS spectrum (Fig. 3B) showed a distinct second peak that was best fitted with a shell of one Fe atom at 2.75 Å, with some contribution from several light atoms (O or N) at 3.07 Å. These light atoms may have been derived from water or protein atoms surrounding the core. The Fe-S and Fe-Fe distances are comparable to the edge-shared FeS_4 tetrahedra of cubane-type clusters such as $[Fe_4S_4(SPh)_4]^{2-}$ (Ph, phenyl) (*15*). However, the occupation number of the Fe coordination shell is significantly lower than values typically required to interpret the Fe K-edge EXAFS of discrete $[Fe_4S_4(SR)_4]^{2-}$ clusters, suggesting that the 500–Fe atom sulfided cores are best described as a disordered array of edge-shared FeS_4 units.

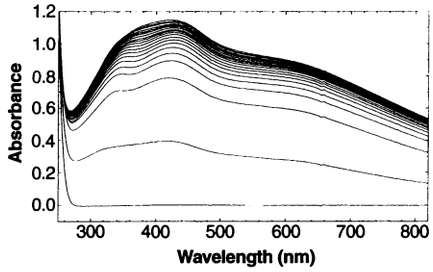

Fig. 1. Ultraviolet-visible spectra showing the in situ sulfidation of native ferritin iron oxide cores. The unreacted ferrihydrite cores show no absorbance in the range 300 to 800 nm. Spectra were recorded at intervals of approximately 7 min with a protein concentration of 10^{-6} M.

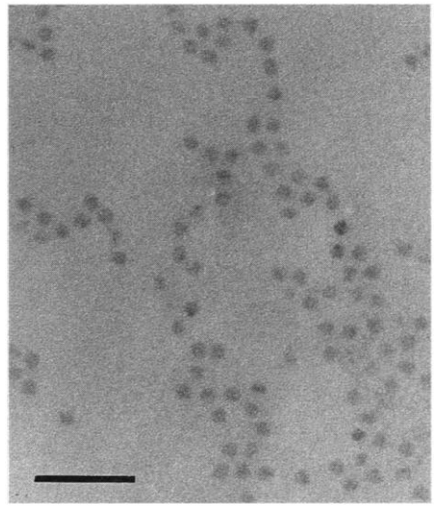

Fig. 2. TEM micrograph showing discrete iron sulfide–ferritin nanocomposites containing approximately 3000 Fe atoms per protein molecule. Scale bar = 40 nm.

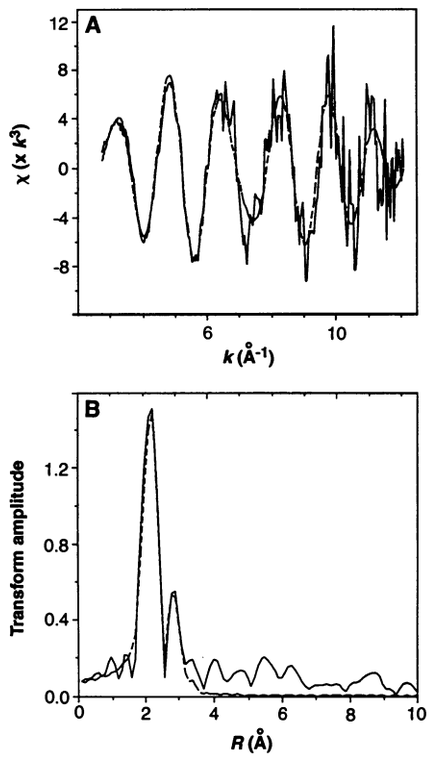

Fig. 3. Iron K-edge EXAFS (**A**) of sulfided reconstituted ferritin containing 500 Fe atoms per molecule (–) and a simulation (····) [backscattering from 4 S, 1 Fe, and 4 O at 2.22, 2.75, and 3.07 Å, respectively, with associated Debye-Waller parameters ($2\sigma^2$) of 0.010, 0.004, and 0.039 Å^2], together with (**B**) their Fourier transforms. In (A), χ is the k^3-weighted EXAFS amplitude, where k is the photoelectron wave vector. The uncertainty in the occupation number of the S shell is estimated as ±1, and the occupation number of the Fe shell is considered to be in the range of 0.5 to 2.0.

Whereas x-ray absorption near-edge structure (XANES) is commonly used for determining metal oxidation states in oxides and other compounds containing "hard ligands," there is no such clear correlation with iron sulfides (*16*). Thus, although the XANES profile observed for the K-edge of the sulfided ferritin sample was consistent with Fe in an environment of S atoms, no unequivocal determination of the formal oxidation state could be obtained by this method. Therefore, we used ^{57}Fe Mössbauer spectroscopy to determine the oxidation state and magnetic properties of the iron sulfide nanocomposites. Spectra obtained at 77 K of the sulfided native ferritin containing 3000 Fe atoms per molecule showed a single quadrupole split doublet with a narrow linewidth (0.27 mm s^{-1}) (Fig. 4A) (*17*). The isomer shift values and quadrupole splitting parameters were 0.28 and 0.38 mm s^{-1}, respectively. These data indicate the presence of an Fe species significantly different from unreacted native ferritin, for which the ferrihydrite cores give isomer shift and quadrupole splitting values at this temperature of about 0.5 and 0.7 mm s^{-1}, respectively (*18*).

The 77 K spectrum of the sulfided ferritin loaded to 500 Fe atoms per molecule was more complex, showing two overlapping quadrupole-split peaks (Fig. 4B). One of these was a relatively narrow doublet (linewidth = 0.39 mm s^{-1}) with isomer shift and quadrupole splitting values of 0.34 and 0.61 mm s^{-1}, respectively; the other was a more broadened doublet (linewidth = 0.52 mm s^{-1}) with isomer shift and quadrupole splitting values of 0.48 and 1.26 mm s^{-1}, respectively. Spectra recorded at 4.2 K showed clear evidence of magnetic ordering (with a mean magnetic hyperfine field of about 26 T) in the 500–Fe atom sulfide cores, whereas the sulfided native ferritin (3000 Fe atoms per molecule) showed only an indication of the onset of magnetic ordering (Fig. 5, A and B). These data, like those

obtained at 77 K, are very different from the parameters determined for unreacted native ferritin; the 4.2 K spectrum for ferritin shows a well-resolved sextet with a magnetic hyperfine field of 49 T.

The isomer shifts of the sulfided samples of native and reconstituted ferritins are too low to correspond to tetrahedral Fe(II) but fall within the established range for high-spin Fe(III) in tetrahedral sites (*19*). Thus, both nanocomposites can be classified as predominantly amorphous ferric sulfides, although the smaller clusters appear to be more structurally and magnetically ordered. The higher values of the quadrupole splitting parameters of the sulfided ferritin containing 500 Fe atoms as compared with those that contain 3000 Fe atoms per molecule could originate from their larger surface-to-volume ratio, which increases the average asymmetry of the environment around each Fe center. Furthermore, the smaller cores contain an additional component (approximately 50%) with a higher quadrupole splitting and isomer shift (0.48 mm s^{-1}) that can be assigned to a tetrahedral Fe center with an effective mean charge of approximately +2.5, suggesting that there is significant mixed-valence character in the 500–Fe atom clusters (*19*, *20*). The nonintegral valency suggests that there is facile delocalization of spin electrons, possibly by superexchange charge transfer through the $Fe(S)_2Fe$ bridges indicated by the EXAFS data. Similar Mössbauer data have been observed for partially reduced states of Fe-S proteins, which also have metallocenters based on edge-shared FeS_4 tetrahedra (*21*), and we speculate that this similarity in the local structure and oxidation state might indicate that the 500–Fe atom ferritin nanocomposite could be utilized in biomolecular reactions involving electron transfer.

The results presented in this report indicate that the reaction of acidic (pH 5.4) sulfide solutions with ferritin results in the in situ nanoscale synthesis of protein-encapsulated iron sulfides. Imaging of the sulfide cores by electron microscopy suggests negligible loss of Fe from the protein cavity during reaction, and electron diffraction, EXAFS analysis, and ^{57}Fe Mössbauer spectroscopy indicate that the transformation of the native oxide is essentially complete. Synthesis of Fe(III) sulfide at the nanometer scale is surprising because most iron sulfides are thought to consist of Fe(II) ions, except for a mixed–oxidation state mineral, greigite (Fe_3S_4) (*22*). However, there are a few reports of an amorphous Fe(III) sulfide, "Fe_2S_3" (*23*). The Mössbauer spectrum of this material at 77 K shows two quadrupole components with isomer shift values very similar to the two components observed in the spectrum of the 500–Fe atom sulfide cores (Fig. 4B), but the quadrupole splitting parameters are very different (*24*).

The key factor determining the extent of reaction in our experiments was the optimization of the rates of reductive dissolution of the ferrihydrite core (low pH) and iron sulfide precipitation (high concentration of S^{2-}). In general, reaction of iron oxides with sulfide proceeds by means of a sequence of steps involving the rapid surface adsorption of sulfide, formation of a surface-bound ferric sulfide, electron transfer, and dissolution of Fe(II) (*25*). At high pH, this pathway is limited by the low solubility of iron sulfides and iron hydroxides; however, it can readily take place under acidic conditions. It appears that negligible reduction of the ferrihydrite core of ferritin occurs under our reaction conditions and that the transformation is promoted simply by solubility differences established by the large excess of sulfide ligands compared with the OH^- concentration. This pathway seems not to be influenced by the reaction environment of the protein cavity [similar chemical procedures in bulk solution in the absence of ferritin also result in the formation of Fe(III) sulfide (*26*)].

Inorganic colloids or sols are used in immunochemistry (Au) (*27*), ulcer treatment (BiO citrate) (*28*), photon emission tomography (^{67}Ga and $^{99m}TcS_2$) (*29*), and magnetic resonance imaging (Fe_3O_4) (*30*). The ability to synthesize nanomaterials within ferritin might provide both the biocompatibility and biosignaling often demanded in these applications. The interactions of bioinorganic nanoparticles with cellular systems and the utilization of their catalytic, redox, and photochemical properties in influencing biological activity and function are principal objectives of future investigations.

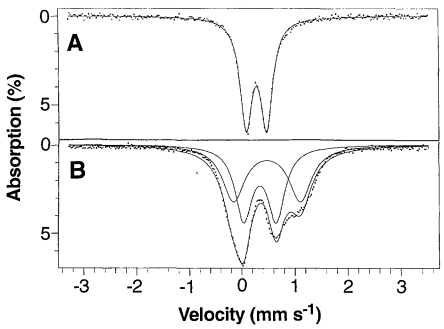

Fig. 4. ^{57}Fe Mössbauer spectra at 77 K of (**A**) sulfided native ferritin (3000 Fe atoms per molecule) and (**B**) sulfided reconstituted ferritin (500 Fe atoms per molecule).

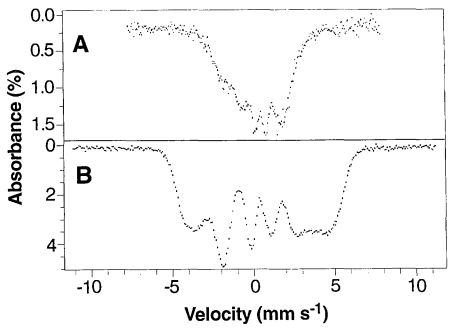

Fig. 5. ^{57}Fe Mössbauer spectra at 4.2 K of (**A**) sulfided native ferritin (3000 Fe atoms per molecule) and (**B**) sulfided reconstituted ferritin (500 Fe atoms per molecule).

REFERENCES AND NOTES

1. G. A. Ozin, *Adv. Mater.* **4**, 612 (1992).
2. S. Mann, *Nature* **365**, 499 (1993).
3. F. C. Meldrum, B. R. Heywood, S. Mann, *Science* **257**, 522 (1992).
4. F. C. Meldrum, V. J. Wade, D. L. Nimmo, B. R. Heywood, S. Mann, *Nature* **349**, 684 (1991).
5. F. C. Meldrum, T. Douglas, S. Levi, P. Arosio, S. Mann, *J. Inorg. Biochem.* **58**, 59 (1995).
6. J. W. M. Bulte *et al.*, *J. Magn. Reson. Imaging* **4**, 497 (1994).
7. J. F. Hainfeld, *Proc. Natl. Acad. Sci. U.S.A.* **89**, 11064 (1992).
8. T. G. St. Pierre, W. Chua-Anusorn, P. Sipos, I. Kron, J. Webb, *Inorg. Chem.* **32**, 4480 (1993).
9. P. Mackle, J. M. Charnock, C. D. Garner, F. C. Meldrum, S. Mann, *J. Am. Chem. Soc.* **115**, 8471 (1993); P. Mackle, C. D. Garner, R. J. Ward, T. J. Peters, *Biochim. Biophys. Acta* **1115**, 145 (1991); J. S. Rohrer, T. I. Quazi, G. D. Watt, D. E. Sayers, E. C. Theil, *Biochemistry* **29**, 259 (1990).
10. Horse spleen ferritin in 0.1 M acetate buffer (pH 5.4) was purged with Ar (or N_2) for ~20 min. Aqueous Na_2S was added to the protein solution such that the sulfide : iron ratio was 5:1. The reaction was stirred for 30 min at pH 5.4 under an inert atmosphere. Then, a further 5 equivalents of Na_2S was added and the reaction was stirred for another hour.
11. J. Zhou *et al.*, *J. Am. Chem. Soc.* **114**, 10843 (1992); P. K. Mascharak, G. C. Papaefthymiou, R. B. Frankel, R. H. Holm, *ibid.* **103**, 6110 (1981). Iron-sulfur cluster compounds often show two absorption maxima, in the region of 340 and 420 nm, considered to be metal-ligand charge-transfer bands. Adopting the extinction coefficients E for a typical synthetic $[Fe_4S_4(SR)_4]^{2-}$ cubane (409 nm, E = 16,000 M^{-1} cm^{-1}; 343 nm, E = 20,000 M^{-1} cm^{-1}) gave values of ~2600 and ~2900 Fe atoms, respectively, for the theoretical metal loading of the sulfided native protein.
12. Samples for TEM were dried onto Formvar-covered, C-coated, Ni TEM grids (3 mm in diameter, 200 mesh) and washed with deaerated water, under an Ar atmosphere, to remove excess sulfide. A Jeol 2000 FX high-resolution analytical electron microscope operating at 200 keV was used.
13. Apoferritin was prepared by thioglycolic acid reduction of horse spleen ferritin (Boehringer Mannheim) [A. Treffry and P. M. Harrison, *Biochem. J.* **171**, 313 (1978)]. The demetallated apoferritin was remineralized to an average core content of 500 Fe atoms by the air oxidation of $(NH_4)_2Fe(SO_4)_2$ (25 mM), added in five aliquots to the protein solution (10^{-6} M) at pH 6.5 in 0.1 M MOPS buffer [I. G. Macara, T. G. Hoy, P. M. Harrison, *Biochem. J.* **126**, 151 (1972)]. The remineralized ferritin was dialyzed against 0.1M acetate buffer (pH 5.4), and the solution was then purged with Ar (or N_2) for ~20 min before reaction with an acidic sulfide solution.
14. Samples for EXAFS were prepared with 10% glycerol to suppress formation of crystalline ice and were maintained at 78 K in a liquid-N_2 cryostat. We recorded spectra on station 8.1 of the Daresbury SRS operating at 2 GeV with an average current of 110 mA, using a Si(111) focusing monochromator and a Canberra 13-element solid-state fluorescence detector. Ten scans were recorded and averaged. We analyzed the isolated data using EXCURV92 [N. Binsted, J. W. Campbell, S. J. Gurman, P. C. Stephenson, *SERC Daresbury Laboratory EXCURV92 Program* (1991)]. We evaluated the single scattering, spherical wave

approximation with phase shifts derived fron ab initio calculations, using Hedin-Lundqvist potentials [P. A. Lee and J. B. Pendry, *Phys. Rev. B* **11**, 2795 (1975)]. The amplitude factor, AFAC in EXCURV92, was taken as 0.7 and not refined. The correction to the energy zero, E_f in EXCURV92, was refined to a value of −5.7 eV. We obtained a theoretical fit by adding shells of the backscattering atoms around the central Fe absorber and iterating the absorber-scatterer distances and Debye-Waller type factors. The latter included contributions from the thermal motion of the absorber-scatterer pairs and a static contribution from any variation in distance between the scatters in one shell. For the first shell only, we also iterated the number of backscatterers to find the best fit. The statistical test described by R. W. Joyner, K. J. Martin, and P. Meehan [*J. Phys. C* **20**, 4005 (1987)] indicated an improvement in the fit index at the 1% significance level on addition of the second shell.

15. B. A. Averill, T. Herskovitz, R. H. Holm, J. A. Ibers, *J. Am. Chem. Soc.* **95**, 3523 (1973).
16. Iron K-edge positions (electron volts) from XANES data: FeS_2 (7.1) FeAsS (6.4), $FeAs_2$ (5.9), $FeCuS_2$ (6.9), Fe_3S_4 (6.7), $(Fe,Ni)_3S_4$ (7.1), $FeCu_5S_4$ (6.9), and amorphous FeS (6.8).
17. We carried out ^{57}Fe Mössbauer spectroscopy using a conventional constant acceleration spectrometer and a ^{57}Co source. We maintained samples at low temperature by using liquid-N_2 and liquid-He bath cryostats. We calibrated the spectra using an Fe metal foil at room temperature and plotted with the center of the Fe metal spectrum as the zero of the velocity axis. Reconstituted ferritin samples for ^{57}Fe Mössbauer spectroscopy were enriched with ^{57}Fe [E. R. Bauminger, P. M. Harrison, I. Nowik, A. Treffry, *Biochemistry* **28**, 5486 (1989)]. The samples were stored frozen in liquid N_2 until used.
18. T. G. St Pierre *et al.*, *Biochim. Biophys. Acta* **870**, 127 (1986); J. M. Williams, D. P. Danson, C. Janot, *Phys. Med. Biol.* **23**, 835 (1978); R. B. Frankel, G. C. Papaefthymiou, G. D. Watt, in *Mössbauer Spectroscopy Applied to Inorganic Chemistry*, vol. 2, G. J. Lond, Ed. (Plenum, New York, 1987), p. 273.
19. J. B. Goodenough and G. A. Fatseas, *J. Solid State Chem.* **41**, 1 (1982). Typical values for the isomer shifts of octahedral high-spin Fe-S compounds are approximately 0.4 mm s^{-1} for Fe(III) and 0.8 mm s^{-1} for Fe(II). Tetrahedral coordination of Fe to S ligand gives isomer shift values of approximately 0.2 mm s^{-1} [Fe(III)], 0.4 mm s^{-1} (Fe +2.5), and 0.6 mm s^{-1} [Fe(II)].
20. An isomer shift value of 0.48 mm s^{-1} could also be interpreted as Fe(III) coordinated to six S atoms within the 500–Fe atom core. However, a typical Fe–S bond length for octahedral geometry is 2.41 Å, which is significantly larger than the experimental value of 2.22 Å determined by EXAFS analysis.
21. R. Cammack, D. P. E. Dickson, C. E. Johnson, *Iron-Sulfur Proteins*, W. Lovenberg, Ed. (Academic Press, New York, 1977), vol. 3, pp. 283–330.
22. J. C. Ward, *Rev. Pure Appl. Chem.* **20**, 175 (1970).
23. R. H. Griffith and A. R. Morcorn, *J. Chem. Soc.* **1945**, 786 (1945); R. Schrader and C. Pietzsch, *Z. Chem.* **8**, 154 (1968).
24. A. H. Stiller, B. J. McCormick, P. Russell, P. A. Montano, *J. Am. Chem. Soc.* **100**, 2554 (1978). The 77 K spectrum of "Fe_2S_3" showed two quadrupole components with isomer shift values of 0.35 and 0.51 mm s^{-1} and with quadrupole splittings of 0.82 and 0.88 mm s^{-1}, respectively. The hyperfine field at 4.2 K was 25 T.
25. D. E. Canfield and R. A. Berner, *Geochim. Cosmochim. Acta* **51**, 645 (1987); W. dos Santos Afonso and W. Stumm, *Langmuir* **8**, 1671 (1992).
26. T. Douglas *et al.*, unpublished observations.
27. J. E. Beesley, *Proc. R. Microsc. Soc.* **20**, 187 (1985).
28. D. W. R. Hall, *Scand. J. Gastroenterol.* **24**, 3 (1989).
29. P. J. Ell and E. S. Williams, *Nuclear Medicine: An Introductory Text* (Blackwell Scientific, Oxford, 1981).
30. T. A. Kent, M. J. Quast, B. J. Kaplan, R. S. Lifsey, H. M. Eisenberg, *Magn. Reson. Med.* **13**, 434 (1990).
31. Postdoctoral support for the work of T.D. was provided by the Engineering and Physical Sciences Research Council, United Kingdom.

9 February 1995; accepted 11 May 1995

Dynamics of Carbonium Ions Solvated by Molecular Hydrogen: $CH_5^+(H_2)_n$ (n = 1, 2, 3)

D. W. Boo, Z. F. Liu, A. G. Suits, J. S. Tse,* Y. T. Lee*

The dynamics of the carbonium ion (CH_5^+), a highly reactive intermediate with no equilibrium structure, was studied by measuring the infrared spectra for internally cold $CH_5^+(H_2)_n$ (n = 1, 2, 3) stored in an ion trap. First-principle molecular dynamics methods were used to directly simulate the internal motion for these ionic complexes. The combined experimental and theoretical efforts substantiated the anticipated scrambling motion in the CH_5^+ core and revealed the effect of the solvent molecular hydrogen in slowing down the scrambling. The results indicate the feasibility of using solvent molecules to stabilize the floppy CH_5^+ ion in order to make it amenable to spectroscopic study.

Protonated alkanes are highly reactive intermediates that form in the acid-catalyzed transformations of hydrocarbons as pioneered by Olah and co-workers (*1*). These carbonium ions are known to form a three-center, two-electron (3c2e) bond, which has pentacoordinated C atoms and bridged H atoms (*2*). The simplest carbonium ion, CH_5^+, has attracted considerable attention from both experimentalists and theoreticians during the last two decades (*3*, *4*). Recent ab initio calculations at the most sophisticated level, performed by Schleyer, Schaefer, and co-workers (*5*), predicted the eclipsed C_s (e-C_s) symmetry to be the global minimum energy structure. However, the calculated energy differences between the e-C_s structure and others, such as the staggered C_s or C_{2v} structures, were very small and became negligible when corrected for zero-point vibrational energies. As emphasized by Scuseria (6, p. 512) recently, these results "clearly indicated that for all practical purposes CH_5^+ does not have a unique, stable equilibrium structure. The hydrogen atoms are predicted to scramble almost freely among multiple equivalent minima."

Studying the dynamics of such internal motion is quite challenging. Fourier transform ion cyclotron resonance mass spectrometry has been used experimentally to characterize indirectly the structure of CH_5^+, but the results were inconclusive (*3*). Many attempts have been made to obtain high-resolution infrared (IR) spectra for CH_5^+, with little success, probably because of the scrambling of CH_5^+ even at low temperatures, which caused significant spectral congestion. Theoretically, elucidation of the scrambling motion in CH_5^+ requires us to go beyond conventional quantum chemistry methods, which essentially treat a molecular or ionic system as a static entity. Molecular dynamics (MD) methods (*7*) would be ideal for such a floppy system, but unfortunately construction of a potential surface for such an ion with strong and complex chemical interactions is an almost impossible task.

We report an attempt to overcome these difficulties by a combination of state-of-the-art experimental and theoretical techniques. These efforts have been directed toward a study of the dynamics of the scrambling motion of core CH_5^+ in molecular hydrogen–solvated carbonium ions, $CH_5^+(H_2)_n$ (n = 1, 2, 3). The motivation was the notion that the interactions between the core CH_5^+ ions and the H_2 molecules are weak enough to cause only a minor perturbation to CH_5^+, yet strong enough to slow down the scrambling motions. Preliminary experimental results on $CH_5^+(H_2)$ (*8*) indicated the extensive scrambling of CH_5^+ and also some slowing of the scrambling by the solvent H_2, but the origin of these phenomena could not be determined because the spectral features were not resolved.

We used ion trap vibrational predissociation spectroscopy to measure the IR absorption of $CH_5^+(H_2)_n$ (n = 1, 2, 3). The experimental setup has been described in detail (*9*). Briefly, internally cold $CH_5^+(H_2)_n$ (n = 1, 2, 3) was produced from a high-pressure and low-current corona discharge source and subsequently was allowed to supersonically expand. The ion source was maintained at the optimum temperature for each kind of cluster ion to maximize the ion intensity. After several stages of ion optics to shape the beam, the ions were mass-selected by a 60° magnet sector analyzer, decelerated to a translation energy of ≤0.5 eV, and focused into a radio-frequency octapole ion trap. The ions were trapped there for ~2 ms, during which time the metastable ions decomposed and some radiative cooling took place for internally hot ions. The trapped, mass-selected ions were then vibrationally excited with a pulsed, tunable IR laser operating

D. W. Boo, Z. F. Liu, A. G. Suits, Y. T. Lee, Department of Chemistry, University of California, Berkeley, CA 94720, USA, and Chemical Sciences Division, Lawrence Berkeley Laboratory, 1 Cyclotron Road, Berkeley, CA 94720, USA.
J. S. Tse, Steacie Institute for Molecular Sciences, National Research Council of Canada, Ottawa, Ontario K1A 0R6, Canada.
*To whom correspondence should be addressed.